Nanoscale

NiFe-Mixed Metal Porphyrin Aerogels as Oxygen Evolution Reaction Catalysts in Alkaline Electrolysers

Journal:	*Nanoscale*
Manuscript ID	NR-ART-10-2022-005675.R1
Article Type:	Paper
Date Submitted by the Author:	06-Nov-2022
Complete List of Authors:	Moschkowitsch, Wenjamin; Bar-Ilan University, Chemistry Samanta, Bipasa; Indian Institute of Technology Bombay Zion, Noam; Bar-Ilan University Faculty of Exact Sciences, Chemistry Honig, Hilah; Bar-Ilan University Faculty of Exact Sciences, Chemistry Cullen, David; Oak Ridge National Laboratory, Materials Science & Technology Division Caspary Toroker, Maytal; Technion, Materials Science and Engineering Elbaz, Lior; Bar-Ilan University Faculty of Exact Sciences, Chemistry

NiFe-Mixed Metal Porphyrin Aerogels as Oxygen Evolution Reaction Catalysts in Alkaline Electrolysers

Wenjamin Moschkowitsch[1,2] Bipasa Samanta[3], Noam Zion[1,2], Hilah C. Honig[1,2], David A. Cullen[4], Maytal Caspary Toroker[2*], Lior Elbaz[1,2*]

[1] Chemistry Department, Bar-Ilan University, Ramat-Gan 5290002, Israel
[2] Bar-Ilan Center for Nanotechnology and Advanced Materials, Bar-Ilan University, Ramat-Gan 5290002, Israel
[3] Department of Materials Science and Engineering and The Nancy and Stephen Grand Technion Energy Program, Technion-Israel Institute of Technology, Haifa 3200003, Israel
[4] Center for Nanophase Materials Sciences, Oak Ridge National Laboratory, Oak Ridge, TN 37831, USA

[*] Corresponding authors: maytalc@technion.ac.il, lior.elbaz@biu.ac.il

Abstract

Aerogels are a very interesting group of materials owing to their unique physical and chemical properties. In the context of electrocatalysis, the focus has been on their physical properties, and they have been used primarily catalyst supports so far. In this work, we synthesized porphyrin aerogels containing Ni and NiFe mixed metal materials and studied them as catalysts for the oxygen evolution reaction (OER). Different Ni:Fe ratios were synthesized and studied in electrochemical cells, and DFT calculations were conducted in order to gain insight into their behavior. The activity trends were dependent on the metal ratios and differ from known NiFeOOH materials due to the change of the oxidation states of the metals to higher numbers. Herein, we show that Ni and Fe have a synergistic effect for OER, despite being structurally separated. They are connected electronically, though, through a large organic aromatic system that facilitates electron sharing between them. In this mixed metal porphyrin aerogels, the best ratio was found to be Ni:Fe = 35:65, in contrast to oxide/oxyhydroxide materials in which a ratio of 80:20 was found to be ideal.

Keywords: electrocatalysis, oxygen evolution reaction, aerogels, PGM free catalysts, alkaline electrolyzers, metal porphyrins, DFT calculations

Introduction

Climate change is one of the most significant challenges of the 21st century.[1, 2] To mitigate its effects, it is necessary to decrease the amount of greenhouse gases (GHG) emitted into the atmosphere.[3] In parallel, the world's population and energy demand are projected to continuously rise in the near future.[4] To reduce GHG emissions while in the face of growing energy demand, new environmentally friendly methods for energy generation and storage must be rapidly developed.[5, 6]

One of the most prominent emerging clean energy technologies is the use of hydrogen rather than fossil fuels as an energy carrier. Hydrogen needs to be produced without emitting GHGs, otherwise the issues relating to them are only shifted.[6] One way to do this is to utilize renewable energies alongside electrochemical water electrolysers.[6] This is done via two distinct electrochemical reactions, the cathodic hydrogen evolution reaction (HER)[7-11] and the anodic oxygen evolution reaction (OER).[11-22]

The HER is considered to be relatively facile. The state-of-the-art catalyst for this reaction is platinum, which is scarce and costly, and the search for viable alternatives of platinum group metal-free (PGM-free) catalysts is ongoing.[9-11] The OER is considered the bottleneck reaction, since it is a four-electron process which has very sluggish kinetics and requires relatively high overpotential to reach suitable current densities (around 10 mA cm^{-2}).[18] Ir and Ru-based catalysts have been considered the benchmark for decades, but in recent years, PGM-free catalysts based on Ni and Fe such as NiFeOOH have been found to outperform the activity of PGMs in alkaline electrolyzers.[19-21, 23, 24] In this class of PGM-free catalysts, it is important to note that Ni and Fe have a synergistic effect and that both metals are necessary to achieve high catalytic activity at relatively low overpotentials.[16, 18, 24-30] Materials with only one of the metals, e.g. NiOOH, have always shown lower performance when compared to bimetallic NiFe catalysts.[23]

The most difficult challenge with NiFeOOH catalysts is their relatively low surface area. In this regard, one class of materials that has been drawing attention in recent years is aerogels.[31] These materials have a very large void volume (> 97%), are highly porous, ultralight, and have an extremely low density. These properties make them very interesting materials

for a variety of applications such as energy storage devices, sensors and catalyst supports.[31-39] Many different materials can be formed into aerogels, like metals or metal oxides but also organic and inorganic molecules.[40-42] Combining these physical properties with an active material will result in a self-standing, all-in-one catalyst/support material.

Herein, we synthesized porphyrin-based aerogels containing Ni and Ni-Fe with various Ni:Fe ratios. All of these catalysts show activity towards OER, with the mixed metal aerogels showing the best performance. To the best of our knowledge these are the first reported metal-organic aerogels that show activity towards OER. The trends of activity differ from the known trends for NiFeOOH and DFT calculations were used to elucidate these differences.

Experimental

Synthesis: Iron 5,10,15,20-(tetra-4-aminophenyl)-porphyrin (FeTAPP) aerogel and free-base 5,10,15,20-(tetra-4-aminophenyl)porphyrin (H_2TAPP) aerogel were synthesized with the same method as was reported in our previous work.[40, 41] Nickel 5,10,15,20-(tetra-4-aminophenyl)porphyrin (NiTAPP) aerogel was synthesized with an analogous method: $NiCl_2 \cdot 6H_2O$ (26 mg) was dissolved in 250 µL DMSO under stirring. Free-base porphyrin, 5,10,15,20-(tetra-4-aminophenyl)porphyrin (TAPP) (10 mg, 98%, PorphyChem) was added to the solution, which was heated to 80°C and stirred for 30 min. Terephthalaldehyde (98%, Alfa Aeser) with a 1:2 molar ratio of -NH_2 to -CHO in DMSO (250 µL) was added as a crosslinker to form the gel. It was heated to 80°C and kept at this temperature for 24 h. Mixed nickel iron 5,10,15,20-(tetra-4-aminophenyl)-porphyrin NiFeTAPP aerogels with Ni:Fe ratios of 50:50, 80:20, and 20:80, respectively, were synthesized by combining the syntheses of the monometallic materials: Two solutions were prepared, in the first $NiCl_2 \cdot 6\ H_2O$ (21 mg, 28 mg, 11 mg, respectively) was dissolved in DMSO (125 µL) and TAPP was added (5 mg, 8 mg, 2 mg, respectively) and for the second solution $FeCl_2 \cdot 4\ H_2O$ (16 mg, 9mg, 18 mg, respectively) was dissolved in DMSO (125 µL) and TAPP (5 mg, 2 mg, 8 mg, respectively) was added. Both solutions were heated and stirred at 80°C for 30 minutes. After that, the solutions were combined and the cross-linker solution (250 µL) was added. The solution was heated at 80°C for 24 h.

The formed gels were covered in DMSO, which was exchanged once a day over the course of several weeks to wash out precursors. After then, the gel was covered in acetone, which was exchanged once a day over the course of one week.

The gels were dried with CO_2 under supercritical conditions in a critical-point dryer (Tousimis 931GL) to form the aerogels.

Characterization: X-ray diffraction (XRD) patternss were measured with a Bruker-AXS D8-Advanced Diffractometer, using CuKα (1.54 Å) radiation. XPS-spectra were conducted with a Thermo Scientific Nexsa spectrometer and XRF spectra were measured with a Horiba XGT 7200 V instrument. High-angle annular dark-field scanning transmission electron microscopy (HAADF-STEM) images were taken in a JEOL NEOARM, operated at 80 kV.

Electrochemical methods: MTAPP aerogels (1 mg) where dispersed in isopropanol (1 mL) and sonicated for 40 minutes. 3 times 5 µL of the slurry were drop casted on a GC electrode, which was previously polished with alumina slurry (0.3 µm and 0.05 µm, successively), and dried in air. CVs were conducted in a standard three-electrode cell made of Teflon (Pine Instruments) with a GC rod as the counter electrode and a reversible hydrogen electrode (RHE) as the reference electrode. CVs were conducted at a scan rate of 50 mV/s and rotation speed of 900 rpm. The rotation is needed to disperse forming oxygen bubbles on the electrode. 1 M KOH (in deionized water; 18.2 MΩ cm) was used as the electrolyte solution, which was degassed with Ar for 30 min prior to measurements. Ar was bubbled at a low rate for all measurements. A Bio-Logic VMP 300 bi-potentiostat was used to control the potential for all experiments. The catalyst was activated by cycling from 1.2 V vs. RHE to 1.55 V vs RHE for 20 cycles prior to measurement from 1.2 to 1.8 V vs. RHE.

Computational calculations: Density functional theory (DFT) calculations using the Vienna ab initio simulation package (VASP) program was performed,[43, 44] using spin polarized calculation with the formalism of Duradev et al.[44] for the transition metal ions. For the effective modelling of DFT+U, U-J terms of 5.5 and 4 for Ni[45-49] and Fe[50, 51] were used, respectively, as reported in literature. Perdew-Burke-Ernzerhof (PBE)[52] exchange-correlation functional of the generalized gradient approximation (GGA) was used. The Projected augmented wave (PAW) potentials[53, 54] include the contribution of core electrons of each atom. The use of the above-mentioned level of theory for porphyrin rings has been used in previous literature and hence chosen here too.[55-59] An energy cut off of 600 eV with KPOINT mesh of 1x1x1 was used. At first, a unit cell of NiTAPP was built and then minimized with energy and force convergence criteria of $1e^{-4}$ eV and -0.03 eV $Å^{-1}$, respectively. Then, the optimized cell was multiplied in the X and Y direction to build the aerogels with three and four porphyrin rings to

represent the required ratio as used in the experiments. In the three-ring system when one of the rings contains Ni and two contain Fe, the required ratio represented is 33:67. Four ring systems with two and three Fe, respectively, have the ratios of 50:50 and 25:75. Due to the large size of the aerogel system and the smaller importance of ligands (as will be demonstrated in the results section), for the multiplied unit cell only single point energy calculation was done. Gaussian smearing was used with symmetry imposition for all calculations.

Results and Discussion

Nickel and nickel-iron 5,10,15,20-(tetra-4-aminophenyl) porphyrin (NiTAPP and Ni_xFe_yTAPP, respectively) aerogels (AG) were synthesized for the first time for this work. TAPP was metalated with the desired metal chloride salt/s, and was used as the monomer for the gel. It was polymerized via a polycondensation reaction of the aminophenyl groups on the porphyrin ring together with an aldehyde cross-linker as shown in **Scheme 1**. The ratio of Ni:Fe can be easily controlled by the amounts of precursors used for the reaction. However, the ratios measured by XRF differ from the amount used during synthesis as shown in **Table 1**, while no impurities by any other metals were detected. This difference can be explained by lower Fe metalation yield than expected and the remaining of some free-base TAPP porphyrins. The gels were supercritically dried using liquid CO_2 and formed reddish-brown aerogels. An image of 5 mg of NiTAPP porphyrin powder and NiTAPP aerogel synthesized from it is shown in **Figure 1**.

XRD diffractions of NiFeTAPP AG 35:65 is shown in **Figure 2**. The diffraction is composed mostly of background noise, as is expected from an aerogel. There are some small peaks at 2θ = 11, 17, 26, 34, 35, 39, 46, 52, and 56°, which correspond to $NiFeO_x$, FeO_x, and oxyhydroxide materials.[18, 27, 60] Judging from their intensity, only small amount of metallic or oxidized metals were left in the aerogel after the synthesis.

Table 1: Ratio of Ni:Fe in MTAPP aerogels.

Ratio Ni:Fe (used for synthesis)	Ratio Ni:Fe (measured with XRF)	Ratio Ni:Fe (used for DFT calculations)
50:50	35:65	33:67
80:20	61:39	50:50
20:80	24:76	25:75

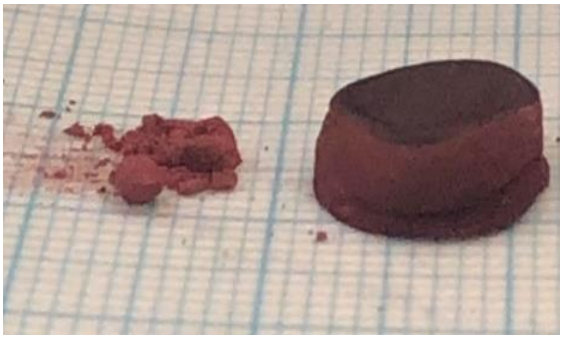

Figure 1: Comparison of NiTAPP powder and NiTAPP aerogel. Both samples in the picture weigh about 5 mg (the pictures were taken on a millimetric paper to give a sense of scale).

The XPS spectra for NiTAPP AG are shown in **Figure S1** and spectra for the mixed metal materials are shown in **Figures S2-4**. The Fe2p XPS spectra look very similar to the ones reported by us for FeTAPP aerogel in the past.[40, 41] The only differences are tiny shifts in the binding energies depending on the Ni:Fe ratios. They are located around 712 and 725 eV in all materials and confirm that Fe is in the oxidation

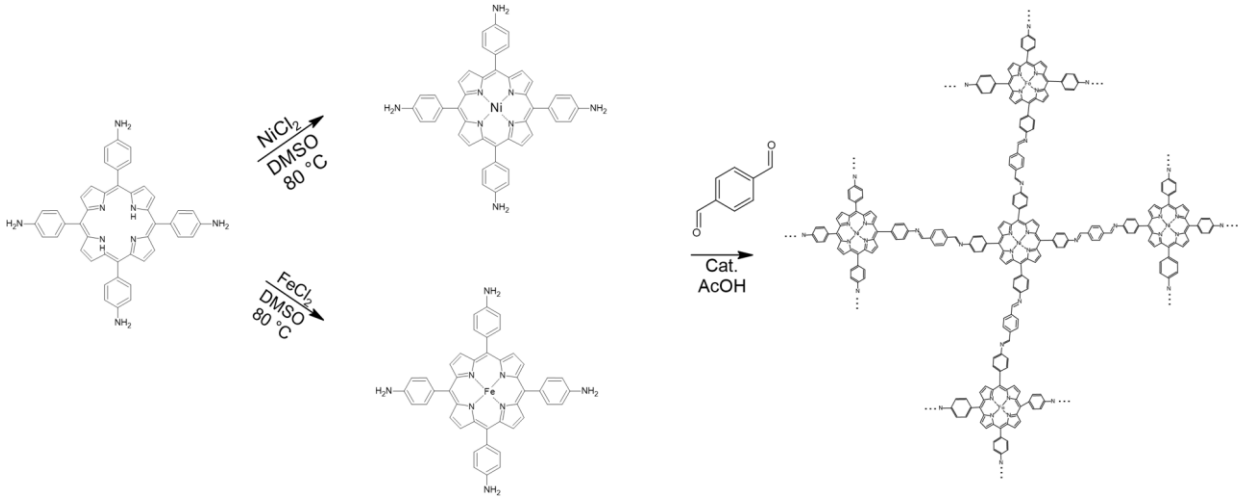

Scheme 1: Synthesis of MTAPP aerogels.

state +3. The Ni2p peaks are located at around 855 and 872 eV and both have small satellite peaks. They show that Ni is in the oxidation state +2. The N1s spectra show peaks for N^{1+} around 401 eV, pyrrolic N around 400 eV, and a large peak for metal-N species around 399 eV. The peaks for N-Ni and N-Fe are located at the same binding energy and could not be distinguished.[61] All the nitrogen peaks agree very well with literature.[62, 63]

HAADF-STEM images of NiFeTAPP AG 35:65 are shown in **Figure 3**. Figure 3A shows a fragment of the porous, 3D covalent framework (COF) on the micrometer scale, as is expected of aerogels. The macrostructure is composed of interconnected flaky sphere-like units. Figure 3B and 3C shows these units with greater magnification. The material appears to have a high degree of micropores and to be very airy. Only insignificant metallic residues were observed, as was expected form XRD measurements.

All synthesized materials show electrocatalytic OER activity in alkaline medium (1 M KOH) as presented in **Figure 4**. The free-base aerogel, devoid of the metals, shows no OER activity, whereas the rest are showing much better activity after the addition of the metals, starting with FeTAPP AG that reaches a bit more than 0.5 mA cm^{-2} at 1.8 V vs. RHE, whereas NiTAPP AG almost goes as high as 1.5 mA cm^{-2} at the same potential. The activity of the mixed Ni_xFe_yTAPP aerogels is around that of the mono-metallic aerogels or higher. NiFeTAPP AG35:65 is the most active reaching 2.8 mA cm^{-2} at 1.8 V vs. RHE, followed by NiFeTAPP AG60:40 with 1.7 mA cm^{-2}, and NiFeTAPP AG24:76 with 0.7 mA cm^{-2} at the same potential. It is important to highlight that the optimum Ni:Fe ratio in the case of these new aerogels is different than in NiFeOOH derived materials, which are known to reach the highest OER activity with an iron content of between 15-25 % and a sharp activity drop when the Fe content increases beyond 50%, whereas in the case of the Ni_xFe_yTAPP aerogels, the best performance was obtained with relatively high Fe

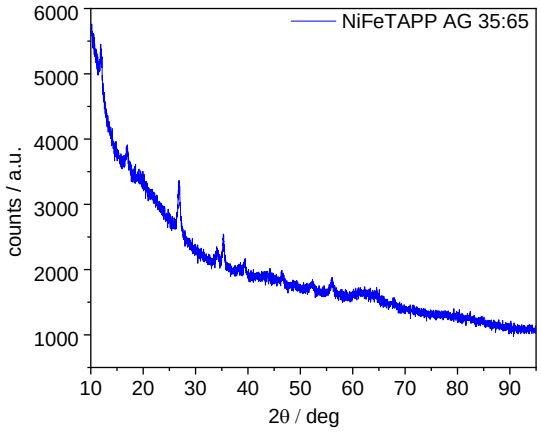

Figure 2: XRD diffraction of NiFeTAPP AG 35:65.

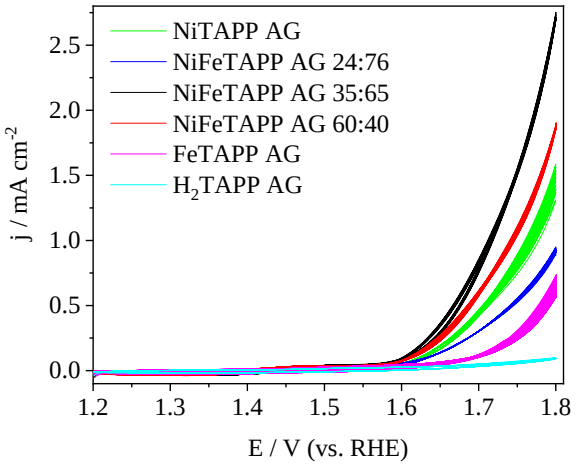

Figure 4: CVs of NiTAPP AG, FeTAPP AG, Ni_xFe_yTAPP AG, and H_2TAPP AG in deaerated 1M KOH solution in DI water (scan rate 50 mV/s).

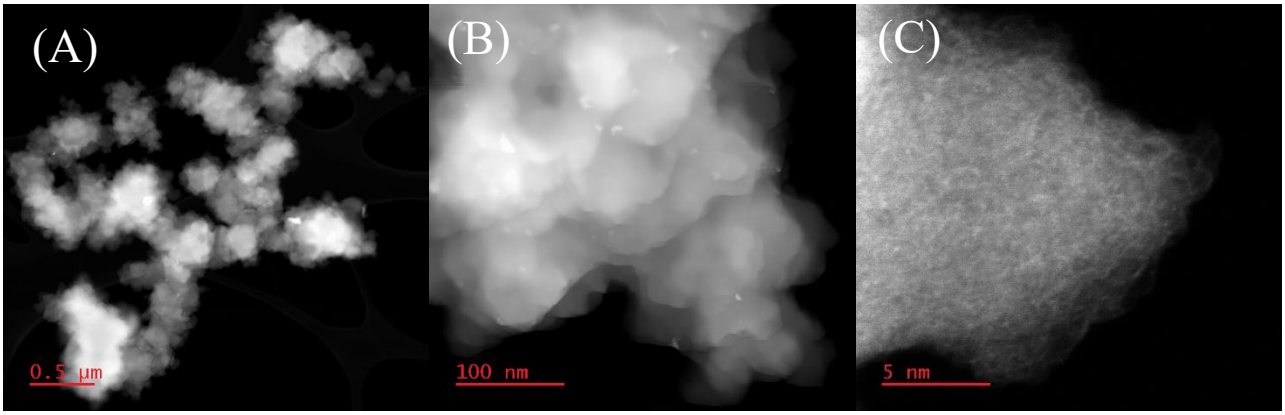

Figure 3: HAADF-STEM images of NiFeTAPP AG35:65 showing (A) interconnected, porous structure, (B) connected polymer structure, and (C) high magnification of aerogel structure.

content.[23, 26, 28] The aerogel with 35:65 Ni:Fe ratio shows higher activity than that of lower Fe content, and a sharp decline in activity appears at an Fe content of 76%.

The fact that the free-base aerogel shows no activity at all, proves that the metals are required to make the aerogels OER active. Previous studies show that Ni-based materials are not very active at all and need Fe dopants to catalyze OER.[23, 64] Here, NiTAPP showed some activity but is outperformed by two mixed metal materials. Purely Fe based materials are not very active as well. It is assumed that synergistic effects of Ni and Fe in certain ratios are necessary for the reaction to execute effectively. This seems to be confirmed here. Similar to NiFeOOH OER catalysts, where the synergistic effects between Ni and Fe were explained by the proximity of these atoms which facilitates electron transfer or sharing between the metals, in the conjugated aromatic TAPP structure, the electrons can move freely, and electron exchange between the different metals can be facilitated as well. Another possible explanation for the high activity of the aerogels is high utilization of active centers, owing to their high surface area and large void volume, which theoretically allows the availability of each possible active site, whereas in the case of crystallite NiFeOOH, significant amounts of the metals are hidden inside the catalyst lattice and not available. Hence, it is possible that the sheer number of available catalytic sites is helping reach this high activity.

The differences in activities between the aerogels can be explained from DFT calculations. The effect of the ligands and linkers was examined. The oxidation state of Ni and the Partial Density of States (PDOS) does not change near the Fermi level when increasing the ligand size (**Figure S5**), which indicates that the electronic structure is affected only by the metal centers.

There are several features in the electronic structure of NiFeTAPP AG33:67 that may explain its good OER activity: (1) low oxidation states of the transition metals which can facilitate easier oxidation, (2) the edge of the valence band is dominated by metal states and therefore oxidation is energetically favorable from the metal states, and (3) low band gap for facile transfer of charge carriers. **Table 2** shows the bandgap values for each system, and **Figure 5** shows the respective PDOS with peaks near the Fermi level. From **Table 2** the Ni:Fe ratio 33:67 indeed has the lowest bandgap of 0.03 eV. From **Figure 5**, a very sharp peak of Fe at the Fermi level was observed, which facilitates easy transfer of electrons for the OER. The observed oxidation states of Ni and Fe are +4 and +2, respectively. Note that the oxidation states are evaluated based on magnetic moment by DFT calculations and the oxidation state of Fe can be either

Table 2: The bandgap values of the aerogel-type systems are represented below. System column represents the aerogel type used to study the particular ratio.

System	Bandgap / eV
Porphyrin (Ni)	1.60
Porphyrin (Ni) with small ligand	1.55
Porphyrin (Ni) with big ligand	1.50
NiTAPP (0 Fe)	1.50
FeTAPP (0 Ni)	1.59
NiFeTAPP (33:67)	0.03
NiFeTAPP (25:75)	0.07
NiFeTAPP (50:50)	0.09

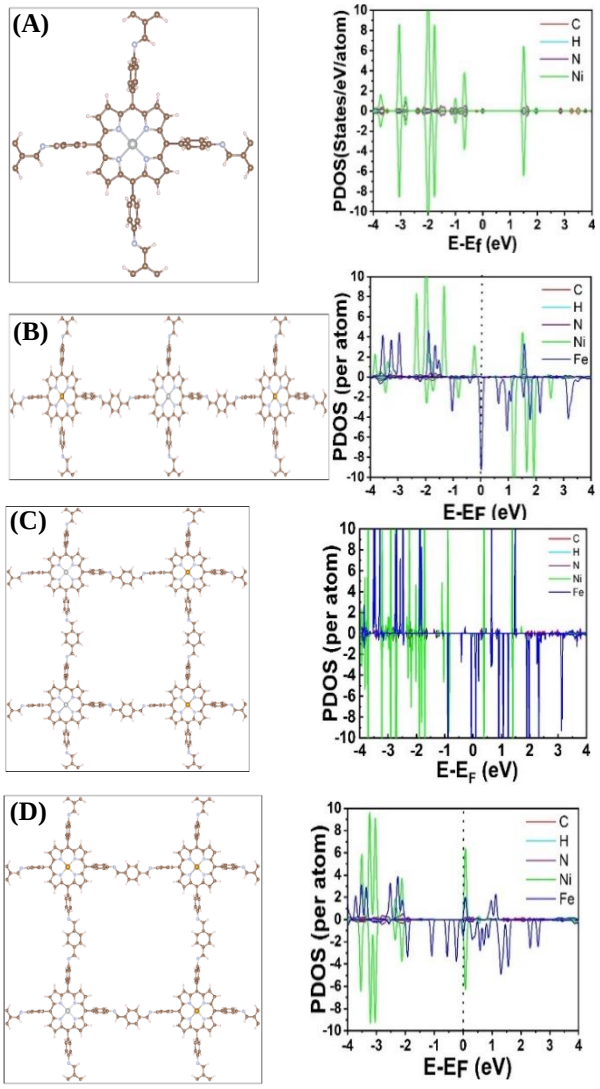

Figure 5: The simulated aerogels structures with the theoretical and experimental ratios, respectively, and corresponding PDOS. (A) Ni unit cell, (B) NiFeTAPP (Ni:Fe = 33:67 ~ 35:65), (C) NiFeTAPP (Ni:Fe = 50:50 ~ 60:40), (D) NiFeTAPP (Ni:Fe = 25:75 ~ 24:76).

+2 or +4, but in any case, must be lower than the oxidation state of Fe in the other NiFeTAPP compounds due to the higher magnetic moment of Fe. Since Fe is in a lower oxidation state, when OER takes place at the Fe center it can increase its oxidation state and can donate electrons easily.

The second-best ratio as found by electrochemical experiments is 60:40, which in computational study was considered close to 50:50. The bandgap observed here is 0.09 eV and there is also a peak of Fe near the Fermi level. The oxidation states of Ni and Fe are +4 and +5, respectively. Since the Fe is already in a high oxidation state, loss of an electron from these centers is difficult and this explains the lower OER activity at this metals ratio. It is similar in the case for 25:75, even though there are Fe peaks near the Fermi level. The oxidation states for Fe are as high as +5 and +6, thus extraction of electrons from the Fe becomes more difficult and the OER activity decreases further, even below the mono NiTAPP material. Moreover, it has been experimentally observed that aerogels with just Fe show lower activity than aerogels with Ni. At high potentials, relevant for OER, the oxidation state of the Fe in the FeTAPP is +4, and for the Ni in NiTAPP is +4 as well. The high oxidation state of Fe does not allow easy electron transfer during OER. Similar is the case of only Ni. Further, for the cases where just Fe or Ni metal ions are present in the porphyrin ring, there is no peak of the metal ion near the Fermi level (**Figure S6**).

At lower potentials (around 1.5 V vs. RHE) the aerogels show a small redox peak which is attributed to the oxidation of Ni^{2+} to $Ni^{3+/4+}$ and is expected of Ni-based materials at these potentials and explains why the calculated oxidation state is higher than the one measured with XPS. An example of such a peak is shown in **Figure S7** in the SI. That peak is not seen in FeTAPP and H_2TAPP aerogels. It is analogous to NiFeOOH based materials where these oxidation levels are necessary to activate the catalysts for the OER. This confirms that electrons can move freely throughout the aromatic system in the ligands and have analogous behavior to NiFeOOH. Hence, structural proximity of the metals is not necessary for the synergistic effect, and that all is needed is a way to facilitate electron sharin/transfer between the metal centers.

Conclusion

NiTAPP and mixed Ni_xFe_yTAPP aerogels were synthesized and characterized for the first time with a modified method to was developed by us previously. All of the materials showed electrocatalytic activity towards OER. The Ni:Fe ratio activity trend is different in the case of porphyrin aerogels when compared to inorganic NiFeOOH derived materials, where, in the former, higher Fe loadings were required in order to reach the highest activity. Different ratios of Ni:Fe in porphyrin aerogels have different bandgaps, metal ion oxidation states, and density of states at the valence band edge. The most influential parameter that may be responsible for the higher activity of NiFeTAPP AG33:67 is the low oxidation state (associated with a higher magnetic moment) of Fe in this specific stoichiometry that can readily allow oxidation for OER. The experimental results were confirmed by DFT calculations and it was shown that the synergistic effects of Ni and Fe in OER catalysis depends on facilitating electron sharing between the metals and not only their structural proximity to each other.

Associated Content

Supporting Information with XPS spectra, additional simulated unit cells, PDOS, and additional electrochemical information available.

Author Contributions:

The manuscript was written through contributions of all authors. All authors have given approval to the final version of the manuscript.

Notes:

The authors declare no competing financial interest

Acknowledgements

The authors would like to thank the Israeli Ministry of Energy for funding this project. This work was conducted in the framework of the Israeli Fuel Cells Consortium. Electron microscopy research was supported by the Center for Nanophase Materials Sciences (CNMS), which is a US Department of Energy, Office of Science User Facility at Oak Ridge National Laboratory.

References

1. Chapman, A.; Itaoka, K.; Hirose, K.; Davidson, F. T.; Nagasawa, K.; Lloyd, A. C.; Webber, M. E.; Kurban, Z.; Managi, S.; Tamaki, T.; Lewis, M. C.; Hebner, R. E.; Fujii, Y., A review of four case studies assessing the potential for hydrogen penetration of the future energy system. *Int. J. Hydrogen Energy* **2019,** *44* (13), 6371-6382.
2. Dincer, I.; Acar, C., Review and evaluation of hydrogen production methods for better sustainability. *Int. J. Hydrogen Energy* **2015,** *40*, 11094-11111.

3. Walter, M. G.; Warren, E. L.; McKone, J. R.; Boettcher, S. W.; Mi, Q.; Santori, E. A.; Lewis, N. S., Solar Water Splitting Cells. *Chem. Rev.* **2010,** *110*, 6446–6473.
4. Kober, T.; Schiffer, H. W.; Densing, M.; Panos, E., Global energy perspectives to 2060 – WEC's World Energy Scenarios 2019. *Energy Strategy Reviews* **2020,** *31*.
5. Holladay, J. D.; Hu, J.; King, D. L.; Wang, Y., An overview of hydrogen production technologies. *Catal. Today* **2009,** *139* (4), 244-260.
6. Gallandat, N.; Romanowicz, K.; Züttel, A., An Analytical Model for the Electrolyser Performance Derived from Materials Parameters. *Journal of Power and Energy Engineering* **2017,** *5*, 34-49.
7. Caban-Acevedo, M.; Stone, M. L.; Schmidt, J. R.; Thomas, J. G.; Ding, Q.; Chang, H. C.; Tsai, M. L.; He, J. H.; Jin, S., Efficient hydrogen evolution catalysis using ternary pyrite-type cobalt phosphosulphide. *Nat Mater* **2015,** *14* (12), 1245-51.
8. Bachvarov, V.; Lefterova, E.; Rashkov, R., Electrodeposited NiFeCo and NiFeCoP alloy cathodes for hydrogen evolution reaction in alkaline medium. *Int. J. Hydrogen Energy* **2016,** *41* (30), 12762-12771.
9. Moschkowitsch, W.; Lori, O.; Elbaz, L., Recent Progress and Viability of PGM-Free Catalysts for Hydrogen Evolution Reaction and Hydrogen Oxidation Reaction. *ACS Catalysis* **2022**, 1082-1089.
10. Zhu, J.; Hu, L.; Zhao, P.; Lee, L. Y. S.; Wong, K. Y., Recent Advances in Electrocatalytic Hydrogen Evolution Using Nanoparticles. *Chem. Rev.* **2020,** *120* (2), 851-918.
11. Moschkowitsch, W.; Gonen, S.; Dhaka, K.; Zion, N.; Honig, H.; Tsur, Y.; Caspary-Toroker, M.; Elbaz, L., Bifunctional PGM-free metal organic framework-based electrocatalysts for alkaline electrolyzers: trends in the activity with different metal centers. *Nanoscale* **2021,** (13), 4576–4584.
12. Dionigi, F.; Zeng, Z.; Sinev, I.; Merzdorf, T.; Deshpande, S.; Lopez, M. B.; Kunze, S.; Zegkinoglou, I.; Sarodnik, H.; Fan, D.; Bergmann, A.; Drnec, J.; Araujo, J. F.; Gliech, M.; Teschner, D.; Zhu, J.; Li, W. X.; Greeley, J.; Cuenya, B. R.; Strasser, P., In-situ structure and catalytic mechanism of NiFe and CoFe layered double hydroxides during oxygen evolution. *Nat Commun* **2020,** *11* (1), 2522.
13. Zaffran, J.; Stevens, M. B.; Trang, C. D. M.; Nagli, M.; Shehadeh, M.; Boettcher, S. W.; Caspary Toroker, M., Influence of Electrolyte Cations on Ni(Fe)OOH Catalyzed Oxygen Evolution Reaction. *Chem. Mater.* **2017,** *29* (11), 4761-4767.
14. Diaz-Morales, O.; Ferrus-Suspedra, D.; Koper, M. T. M., The importance of nickel oxyhydroxide deprotonation on its activity towards electrochemical water oxidation. *Chem Sci* **2016,** *7* (4), 2639-2645.
15. Diaz-Morales, O.; Ledezma-Yanez, I.; Koper, M. T. M.; Calle-Vallejo, F., Guidelines for the Rational Design of Ni-Based Double Hydroxide Electrocatalysts for the Oxygen Evolution Reaction. *ACS Catalysis* **2015,** *5* (9), 5380-5387.
16. Friebel, D.; Louie, M. W.; Bajdich, M.; Sanwald, K. E.; Cai, Y.; Wise, A. M.; Cheng, M. J.; Sokaras, D.; Weng, T. C.; Alonso-Mori, R.; Davis, R. C.; Bargar, J. R.; Norskov, J. K.; Nilsson, A.; Bell, A. T., Identification of highly active Fe sites in (Ni,Fe)OOH for electrocatalytic water splitting. *J. Am. Chem. Soc.* **2015,** *137* (3), 1305-13.
17. Fabbri, E.; Habereder, A.; Waltar, K.; Kötz, R.; Schmidt, T. J., Developments and perspectives of oxide-based catalysts for the oxygen evolution reaction. *Catal. Sci. Technol.* **2014,** *4* (11), 3800-3821.
18. Dionigi, F.; Strasser, P., NiFe-Based (Oxy)hydroxide Catalysts for Oxygen Evolution Reaction in Non-Acidic Electrolytes. *Advanced Energy Materials* **2016,** *6* (23), 1600621.
19. Batchellor, A. S.; Boettcher, S. W., Pulse-Electrodeposited Ni–Fe (Oxy)hydroxide Oxygen Evolution Electrocatalysts with High Geometric and Intrinsic Activities at Large Mass Loadings. *ACS Catalysis* **2015,** *5* (11), 6680-6689.
20. Enman, L. J.; Burke, M. S.; Batchellor, A. S.; Boettcher, S. W., Effects of Intentionally Incorporated Metal Cations on the Oxygen Evolution Electrocatalytic Activity of Nickel (Oxy)hydroxide in Alkaline Media. *ACS Catalysis* **2016,** *6* (4), 2416-2423.
21. Moschkowitsch, W.; Dhaka, K.; Gonen, S.; Attias, R.; Tsur, Y.; Caspary Toroker, M.; Elbaz, L., Ternary NiFeTiOOH Catalyst for the Oxygen Evolution Reaction: Study of the Effect of the Addition of Ti at Different Loadings. *ACS Catalysis* **2020**, 4879-4887.
22. Attias, R.; Vijaya Sankar, K.; Dhaka, K.; Moschkowitsch, W.; Elbaz, L.; Caspary Toroker, M.; Tsur, Y., Optimization of Ni-Co-Fe-Based Catalysts for Oxygen Evolution Reaction by Surface and Relaxation Phenomena Analysis. *ChemSusChem* **2021,** *14* (7), 1737-1746.
23. Trotochaud, L.; Young, S. L.; Ranney, J. K.; Boettcher, S. W., Nickel-iron oxyhydroxide

oxygen-evolution electrocatalysts: the role of intentional and incidental iron incorporation. *J. Am. Chem. Soc.* **2014,** *136* (18), 6744-53.
24. Gorlin, M.; Chernev, P.; Ferreira de Araujo, J.; Reier, T.; Dresp, S.; Paul, B.; Krahnert, R.; Dau, H.; Strasser, P., Oxygen Evolution Reaction Dynamics, Faradaic Charge Efficiency, and the Active Metal Redox States of Ni-Fe Oxide Water Splitting Electrocatalysts. *J. Am. Chem. Soc.* **2016,** *138* (17), 5603-14.
25. Gong, M.; Dai, H., A mini review of NiFe-based materials as highly active oxygen evolution reaction electrocatalysts. *Nano Research* **2014,** *8* (1), 23-39.
26. Landon, J.; Demeter, E.; İnoğlu, N.; Keturakis, C.; Wachs, I. E.; Vasić, R.; Frenkel, A. I.; Kitchin, J. R., Spectroscopic Characterization of Mixed Fe–Ni Oxide Electrocatalysts for the Oxygen Evolution Reaction in Alkaline Electrolytes. *ACS Catalysis* **2012,** *2* (8), 1793-1801.
27. Gorlin, M.; Chernev, P.; Paciok, P.; Tai, C. W.; Ferreira de Araujo, J.; Reier, T.; Heggen, M.; Dunin-Borkowski, R.; Strasser, P.; Dau, H., Formation of unexpectedly active Ni-Fe oxygen evolution electrocatalysts by physically mixing Ni and Fe oxyhydroxides. *Chem Commun (Camb)* **2019,** *55* (6), 818-821.
28. Chen, J. Y.; Dang, L.; Liang, H.; Bi, W.; Gerken, J. B.; Jin, S.; Alp, E. E.; Stahl, S. S., Operando Analysis of NiFe and Fe Oxyhydroxide Electrocatalysts for Water Oxidation: Detection of Fe(4)(+) by Mossbauer Spectroscopy. *J. Am. Chem. Soc.* **2015,** *137* (48), 15090-3.
29. Bates, M. K.; Jia, Q.; Doan, H.; Liang, W.; Mukerjee, S., Charge-Transfer Effects in Ni–Fe and Ni–Fe–Co Mixed-Metal Oxides for the Alkaline Oxygen Evolution Reaction. *ACS Catalysis* **2015,** *6* (1), 155-161.
30. Xiao, H.; Shin, H.; Goddard, W. A. I., Synergy between Fe and Ni in the optimal performance of (Ni,Fe)OOH catalysts for the oxygen evolution reaction. *Proc Natl Acad Sci U S A* **2018,** *115* (23), 5872-5877.
31. Lee, J.-H.; Park, S.-J., Recent advances in preparations and applications of carbon aerogels: A review. *Carbon* **2020,** *163*, 1-18.
32. Smirnova, I.; Gurikov, P., Aerogels in Chemical Engineering: Strategies Toward Tailor-Made Aerogels. *Annu Rev Chem Biomol Eng* **2017,** *8*, 307-334.
33. Zion, N.; Douglin, J. C.; Cullen, D. A.; Zelenay, P.; Dekel, D. R.; Elbaz, L., Porphyrin Aerogel Catalysts for Oxygen Reduction Reaction in Anion-Exchange Membrane Fuel Cells. *Advanced Functional Materials* **2021,** *31* (24), 2100963.
34. Peles-Strahl, L.; Zion, N.; Lori, O.; Levy, N.; Bar, G.; Dahan, A.; Elbaz, L., Bipyridine Modified Conjugated Carbon Aerogels as a Platform for the Electrocatalysis of Oxygen Reduction Reaction. *Advanced Functional Materials* **2021,** *31* (26), 2100163.
35. Zion, N.; Cullen, D. A.; Zelenay, P.; Elbaz, L., Heat-Treated Aerogel as a Catalyst for the Oxygen Reduction Reaction. *Angewandte Chemie International Edition* **2020,** *59* (6), 2483-2489.
36. Elbaz, L.; Korin, E.; Soifer, L.; Bettelheim, A., Evidence for the Formation of Cobalt Porphyrin-Quinone Complexes Stabilized at Carbon-Based Surfaces Toward the Design of Efficient Non-Noble-Metal Oxygen Reduction Catalysts. *Journal of Physical Chemistry Letters* **2010,** *1* (1), 398-401.
37. Elbaz, L.; Korin, E.; Soifer, L.; Bettelheim, A., Mediation at High Potentials for the Reduction of Oxygen to Water by Cobalt Porphyrin--Quinone Systems in Porous Aerogel Carbon Electrodes. *Journal of the Electrochemical Society* **2010,** *157* (1), B27-B31.
38. Elbaz, L.; Korin, E.; Soifer, L.; Bettelheim, A., Electrocatalytic oxygen reduction by Co(III) porphyrins incorporated in aerogel carbon electrodes. *Journal of Electroanalytical Chemistry* **2008,** *621* (1), 91-96.
39. Moschkowitsch, W.; Lori, O.; Elbaz, L., Recent Progress and Viability of PGM-Free Catalysts for Hydrogen Evolution Reaction and Hydrogen Oxidation Reaction. *ACS Catalysis* **2022,** *12* (2), 1082-1089.
40. Zion, N.; Douglin, J. C.; Cullen, D. A.; Zelenay, P.; Dekel, D. R.; Elbaz, L., Porphyrin Aerogel Catalysts for Oxygen Reduction Reaction in Anion-Exchange Membrane Fuel Cells. *Adv. Funct. Mater.* **2021**, 2100963.
41. Zion, N.; Cullen, D. A.; Zelenay, P.; Elbaz, L., Heat-Treated Aerogel as a Catalyst for the Oxygen Reduction Reaction. *Angew. Chem. Int. Ed. Engl.* **2020,** *59* (6), 2483-2489.
42. Peles-Strahl, L.; Zion, N.; Lori, O.; Levy, N.; Bar, G.; Dahan, A.; Elbaz, L., Bipyridine Modified Conjugated Carbon Aerogels as a Platform for the Electrocatalysis of Oxygen Reduction Reaction. *Adv. Funct. Mater.* **2021**, 2100163.
43. Dudarev, S. L.; Botton, G. A.; Savrasov, S. Y.; Humphreys, C. J.; Sutton, A. P., Electron-Energy-Loss Spectra and the Structural Stability of Nickel Oxide: an LSDA+U Study. *Phys. Rev.*

B: Condens. Matter Mater. Phys. **1998,** *57*, 1505−1509.
44. G. Kresse , J. F., Efficiency of ab-initio total energy calculations for metals and semiconductors using a plane-wave basis set. *Comput. Mater. Sci.* **1996,** *6*, 15-50.
45. Li, Y. F.; Selloni, A., Mosaic Texture and Double c-Axis Periodicity of beta-NiOOH: Insights from First-Principles and Genetic Algorithm Calculations. *J Phys Chem Lett* **2014,** *5* (22), 3981-5.
46. Li, Y.-F.; Selloni, A., Mechanism and Activity of Water Oxidation on Selected Surfaces of Pure and Fe-Doped NiOx. *ACS Catalysis* **2014,** *4* (4), 1148-1153.
47. Tkalych, A. J.; Yu, K.; Carter, E. A., Structural and Electronic Features of β-Ni(OH)2 and β-NiOOH from First Principles. *The Journal of Physical Chemistry C* **2015,** *119* (43), 24315-24322.
48. Fidelsky, V.; Caspary Toroker, M., Engineering Band Edge Positions of Nickel Oxyhydroxide through Facet Selection. *The Journal of Physical Chemistry C* **2016,** *120* (15), 8104-8108.
49. Zaffran, J.; Caspary Toroker, M., Benchmarking Density Functional Theory Based Methods To Model NiOOH Material Properties: Hubbard and van der Waals Corrections vs Hybrid Functionals. *J Chem Theory Comput* **2016,** *12* (8), 3807-12.
50. Wang, L.; Maxisch, T.; Ceder, G., Oxidation energies of transition metal oxides within the GGA + U Framework. *Physical Review B* **2006,** *73* (19), 195107.
51. Ding, H.; Virkar, A. V.; Liu, M.; Liu, F., Suppression of Sr surface segregation in La1−xSrxCo1−yFeyO3−δ: a first principles study. *PCCP* **2013,** *15* (2), 489-496.
52. Perdew, J. P.; Burke, K.; Ernzerhof, M., Generalized Gradient Approximation Made Simple. *Phys. Rev. Lett.* **1996,** *77* (16), 3865.
53. Blöchl, P. E., Projector augmented-wave method. *Phys Rev B Condens Matter* **1994,** *50* (24), 17953-17979.
54. Kresse, G.; Joubert, D., From ultrasoft pseudopotentials to the projector augmented-wave method. *Phys. Rev. B* **1999,** *59* (3), 1758.
55. Panchmatia, P. M.; Ali, M. E.; Sanyal, B.; Oppeneer, P. M., Halide Ligated Iron Porphines: A DFT+U and UB3LYP Study. *The Journal of Physical Chemistry A* **2010,** *114* (51), 13381-13387.
56. Panchmatia, P. M.; Sanyal, B.; Oppeneer, P. M., GGA+U modeling of structural, electronic, and magnetic properties of iron porphyrin-type molecules. *Chem. Phys.* **2008,** *343* (1), 47-60.
57. Leung, K.; Nielsen, I. M. B.; Sai, N.; Medforth, C.; Shelnutt, J. A., Cobalt−Porphyrin Catalyzed Electrochemical Reduction of Carbon Dioxide in Water. 2. Mechanism from First Principles. *The Journal of Physical Chemistry A* **2010,** *114* (37), 10174-10184.
58. Hasija, V.; Patial, S.; Raizada, P.; Aslam Parwaz Khan, A.; Asiri, A. M.; Van Le, Q.; Nguyen, V.-H.; Singh, P., Covalent organic frameworks promoted single metal atom catalysis: Strategies and applications. *Coord. Chem. Rev.* **2022,** *452*, 214298.
59. Wende, H.; Bernien, M.; Luo, J.; Sorg, C.; Ponpandian, N.; Kurde, J.; Miguel, J.; Piantek, M.; Xu, X.; Eckhold, P.; Kuch, W.; Baberschke, K.; Panchmatia, P. M.; Sanyal, B.; Oppeneer, P. M.; Eriksson, O., Substrate-induced magnetic ordering and switching of iron porphyrin molecules. *Nature Materials* **2007,** *6* (7), 516-520.
60. Nakahira, A.; Kubo, T.; Murase, H., Synthesis of LDH-Type Clay Substituted With Fe and Ni Ion for Arsenic Removal and Its Application to Magnetic Separation. *IEEE Transactions on Magnetics* **2007,** *43* (6), 2442-2444.
61. Gang, Y.; Pan, F.; Fei, Y.; Du, Z.; Hu, Y. H.; Li, Y., Highly Efficient Nickel, Iron, and Nitrogen Codoped Carbon Catalysts Derived from Industrial Waste Petroleum Coke for Electrochemical CO2 Reduction. *ACS Sustainable Chemistry & Engineering* **2020,** *8* (23), 8840-8847.
62. Shalom, M.; Ressnig, D.; Yang, X.; Clavel, G.; Fellinger, T. P.; Antonietti, M., Nickel nitride as an efficient electrocatalyst for water splitting. *Journal of Materials Chemistry A* **2015,** *3* (15), 8171-8177.
63. Liu, B.; He, B.; Peng, H. Q.; Zhao, Y.; Cheng, J.; Xia, J.; Shen, J.; Ng, T. W.; Meng, X.; Lee, C. S.; Zhang, W., Unconventional Nickel Nitride Enriched with Nitrogen Vacancies as a High-Efficiency Electrocatalyst for Hydrogen Evolution. *Adv Sci (Weinh)* **2018,** *5* (8), 1800406.
64. Klaus, S.; Cai, Y.; Louie, M. W.; Trotochaud, L.; Bell, A. T., Effects of Fe Electrolyte Impurities on Ni(OH)2/NiOOH Structure and Oxygen Evolution Activity. *The Journal of Physical Chemistry C* **2015,** *119* (13), 7243-7254.